

# I. Inverse Compton origin of pulsar $\gamma$ -ray emission. II. Reconnection model of Crab flares.

Maxim Lyutikov<sup>1,\*</sup>

Department of Physics, Purdue University, 525 Northwestern Avenue, West Lafayette, IN 47907-2036

The dates of receipt and acceptance should be inserted later

I. There is growing evidence that pulsars' high energy emission is generated via Inverse Compton mechanism.  
II. The particles producing Crab flares, and possibly most of the Crab Nebula's high energy emission, are accelerated via reconnection events, and not at shock via Fermi mechanisms.

© 0000 WILEY-VCH Verlag GmbH & Co. KGaA, Weinheim

## 1 PULSAR $\gamma$ -RAY EMISSION

Conventionally,  $\gamma$ -ray from pulsars were attributed to incoherent curvature radiation. The detection of the Crab pulsar by VERITAS (VERITAS Collaboration & Aliu, 2011), Fig. 1, and the implied importance of inverse Compton (IC) scattering for the production of  $\gamma$ -ray photons (Lyutikov et al., 2012) signifies a paradigm shift in the study of pulsar high-energy emission. Most models of the underlying physical processes have to be re-evaluated (the geometrical models remain valid.) The importance of the IC scattering makes distinct predictions as to the observed properties of pulsar high-energy emission.

One can derive a very general upper limit, independent of the particular details of the acceleration mechanism, on the possible energy of curvature photons (following a similar approach applicable to synchrotron emission de Jager et al., 1996; Lyutikov, 2010). Assuming that the radius of curvature  $R_c$  of the magnetic field lines is a fraction  $\xi$  of the light cylinder radius  $R_c = \xi R_{LC}$  and balancing acceleration by electric field of the fraction of the magnetic field,  $E = \eta B$  and radiative losses one can find the maximum energy of curvature emission within the Crab pulsar magnetosphere  $\epsilon_{br} = 150 \text{ GeV } \eta^{3/4} \sqrt{\xi}$ . The possibility that the emission above the break energy is produced as a tail to the curvature emission is excluded by the fact that the spectrum of Crab pulsar reported by VERITAS *does not show the exponential cut-off* indicative of the radiation reaction-limited curvature emission.

Reanalyzing the Fermi spectra of the Geminga pulsar above the break, Lyutikov (2012) found that it is well ap-

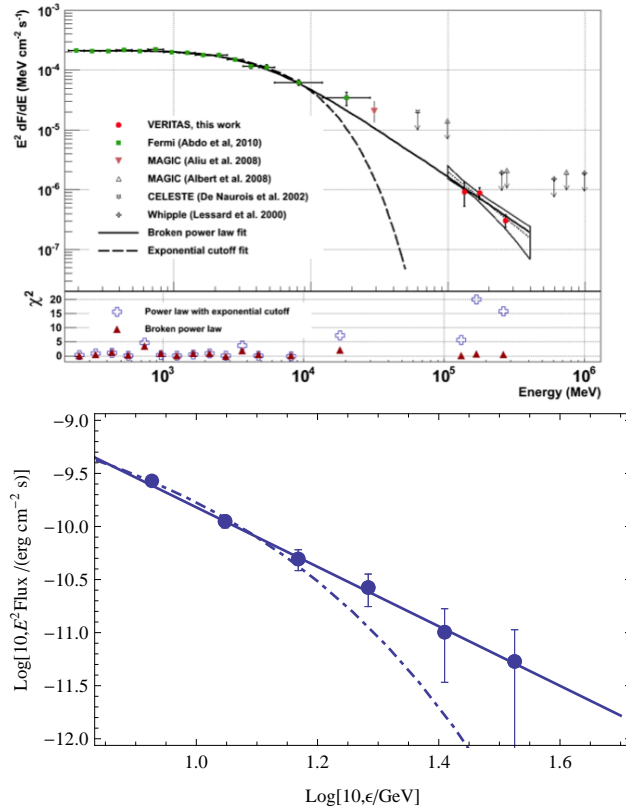


**Fig. 1** Above. Spectral energy distribution of the Crab pulsar VERITAS Collaboration & Aliu (2011). Below. Fits to the high energy tail of the Geminga spectrum: power law (solid line) and exponential cut-off (dashed line) Lyutikov (2012). In both cases the high energy part of the spectrum is power-law, inconsistent with curvature mechanism.

proximated by a simple power law without the exponential cut-off, making Geminga's spectrum similar to that of Crab, Fig. 1. Vela's broadband  $\gamma$ -ray spectrum is equally well fit with both the exponential cut-off and the double power law shapes. In the broadband double power-law fits, for a typical Fermi spectrum of a bright  $\gamma$ -ray pulsar, most of the errors accumulate due to the *arbitrary* parametrization of the spectral roll-off. Thus, based on the data from the first pulsar catalogue, *out of three brightest  $\gamma$ -ray pulsars, the spectra of two (Crab and Geminga) are inconsistent with the exponential cut-off, while the third (Vela) is consistent with double power-law.*

Lyutikov et al. (2012) demonstrated that Inverse Compton scattering by the secondary particles in a Klein-Nishina regime is broadly consistent with the overall energetics and emitted spectra. Klein-Nishina reduction in the scattering cross-section (and the corresponding reduction of the electron energy loss rate) allows the primary leptons to be accelerated to very high energies with hard spectra. The secondary plasma is less energetic but more dense and has approximately the same energy content as the primary beam, producing Synchrotron-Self-Compton radiation. The synchrotron component has a broad peak in the UV-X-ray

\* Corresponding author: e-mail: lyutikov@purdue.edu

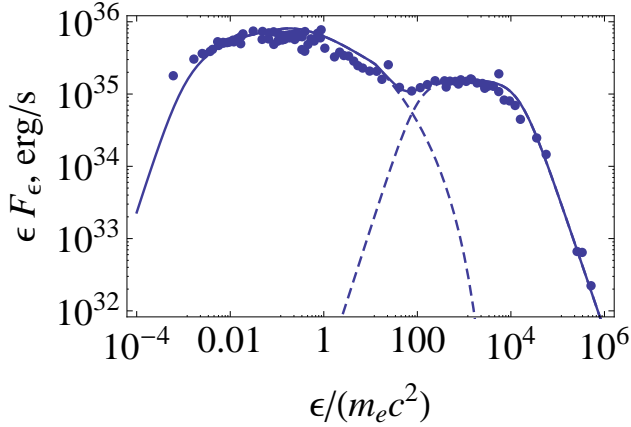


**Fig. 2** The broadband spectrum of the Crab approximated with the CSC model (Lyutikov, 2013). The IC bump in the KN regime provides a direct measurement of the bulk particle distribution, while the high energy part of cyclotron bump constrains the very high energy tail of the particle distribution. **This is a fit over nearly ten decades in energy, using only a handful of parameters.**

range, while the IC component extends to hundreds of GeV. Below  $\sim 1$  GeV the curvature emission from the primary beam can contribute a substantial flux fraction. The IC emission from the primary beam extends well into the TeV regime but can hardly be detected by the ground Cherenkov telescopes.

The model determines the time and phase averaged outcome of the complicated pair production and acceleration processes. Typical Lorentz factor turn out to be  $\gamma \sim$  thousands, which is very reasonable Harding & Muslimov (1998). The only difference with the conventional view is high plasma multiplicity,  $\lambda \sim 10^6 - 10^7$ , but, recall, that Crab nebula needs  $\lambda \sim 10^6$  on average. The procedure to determine the particle spectrum from the observed photon spectrum can be fully numerical (without, *e.g.*, assumption of a power law), with some non-analytical result (in KN regime particle spectrum is easily related to the photon spectrum).

Our results indicate (Lyutikov, 2013) that the broadband spectrum of Crab pulsar, from UV to very high energy gamma-rays - nearly ten decades in energy - can be reproduced within the framework of the cyclotron-self-Compton model. Emission is produced by two counter-streaming beams within the outer gaps, at distances above  $\sim 20$  NS radii. The outward moving beam produces UV-X-ray photons via Doppler-booster cyclotron emission, and GeV photons by Compton scattering the cyclotron photons produced by the inward going beam. The scattering occurs in the deep Klein-Nishina regime, whereby the IC component provides a direct measurement of particle distribution within the magnetosphere. The required plasma multiplicity is high,  $\sim 10^6 - 10^7$ , but is consistent with the average particle flux injected into the pulsar wind nebula, Figs. 2.

There are indications in the second Fermi-LAT catalogue that at high energies pulsar spectra are described better by the power law, and the exponential cut-off spectral shape, 3.

#### Scaling of $\gamma$ -ray luminosity with spin-down power.

Commonly, the  $\gamma$ -ray luminosity is thought to scale with the available potential, which is the square root of the spin-down luminosity, *i.e.*  $\propto \sqrt{\dot{E}}$ . Lyutikov & Otte (2010) demonstrated that *in the radiation reaction-limited regime, the very high energy luminosity is proportional to the spin-down luminosity*:

$$L_\gamma = \eta \eta_G \frac{B_{NS}^2 R_{NS}^6 \Omega^4}{2\pi c^3} = \eta \eta_G \dot{E} \quad (1)$$

where  $\eta_G$  is the volume fraction occupied by the outer gaps, in terms of the light cylinder volume. Recall, that the square-root scaling comes from the assumption (initially appropriately used in the polar cap models of pulsar  $\gamma$ -ray emission) of a potential-limited energy of accelerated particles, that most of this energy is radiated away, and that the particle flux is of the order of the Goldreich-Julian density,  $\dot{N} \propto n_{GJ} r_{PC}^2 \propto \sqrt{\dot{E}}$  (see *e.g.*, Zhang & Harding, 2000). In contrast, in a radiation-limited regime, and assuming that the emitting volume is proportional to the volume within the light cylinder radius, one obtains  $L_\gamma \propto \dot{E}$  (Lyutikov & Otte, 2011), Fig. 4. The estimate (1) of the  $\gamma$ -ray luminosity does not depend on the particular radiation mechanism that limits the particle energy; it will be the same estimate if, *e.g.*, curvature losses or IC scattering in the Thompson regime provide the dominant drag on the particle. On the other hand, it is not really applicable if the sole radiative loss mechanism is the IC scattering in KN regime. In this case the radiative losses are independent of the particle energy, so that the acceleration by the electric field cannot be balanced in a general case by the radiative losses.

**Two photon pair production in outer gaps.** The models of the pulsar magnetospheres are mostly based on the Ruderman & Sutherland (1975) model of pair production near the polar caps. It was then expected that polar cap regions are intense sources of high energy emission (Daugherty & Harding, 1982). These expectations are not supported by few years of *Fermi* data, no gamma-ray emission from pulsar polar caps have been observed. On the other hand, the Crab nebula X-ray emission requires a huge flux of particles, with the *average* over the open field lines multiplicity of  $\langle \lambda \rangle \sim 10^6$ . Thus, there is a contradiction between polar cap pair production models and observations. The importance of Compton scattering in the Klein-Nishina regime implies the importance of pair production in the outer gaps: the corresponding cross-sections are very similar. We will investigate whether a self-consistent model of particle acceleration and pair production in the gaps leads to a stationary particle distribution (this is a highly non-linear electrodynamic problem).

**Expected X-ray- $\gamma$ -ray correlation.** Since the IC power is related to the power of the seed photons, we might expect some  $\gamma$ -ray - soft X-ray correlation. Though it is the

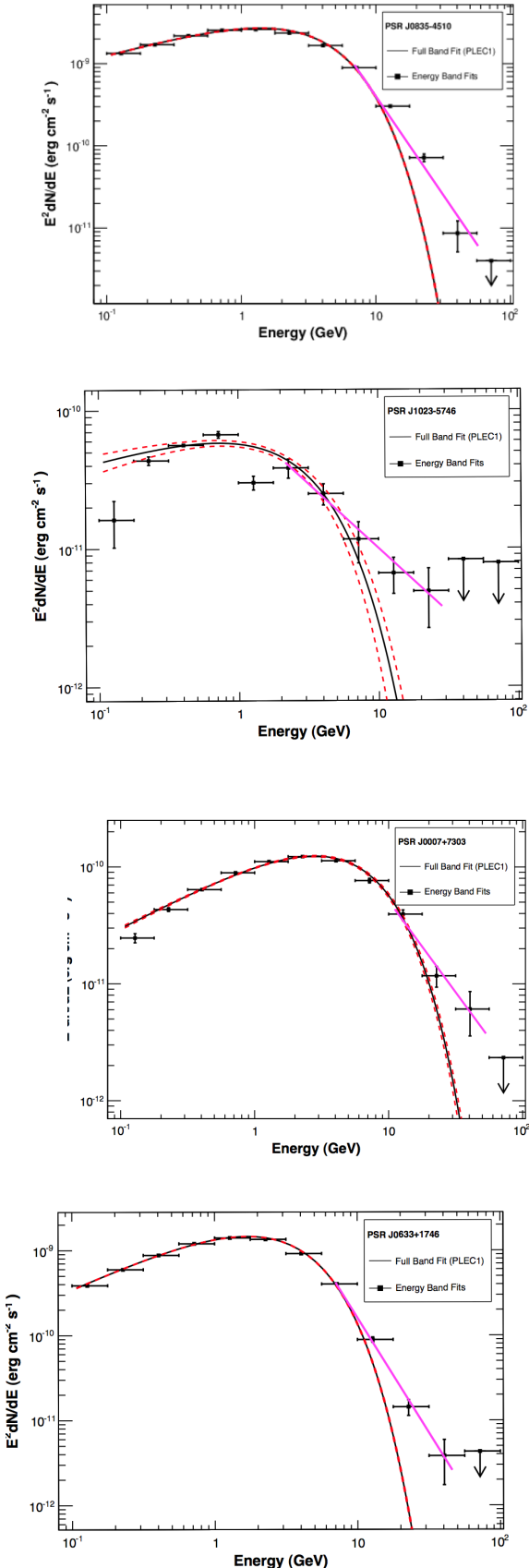


**Fig. 3** Example of pulsar spectra from the second Fermi-LAT catalogue indicative of high energy power-law tails. Red lines: power law plus exponential fits (The Fermi-LAT collaboration, 2013), magenta lines: power law fits for high energy tails.

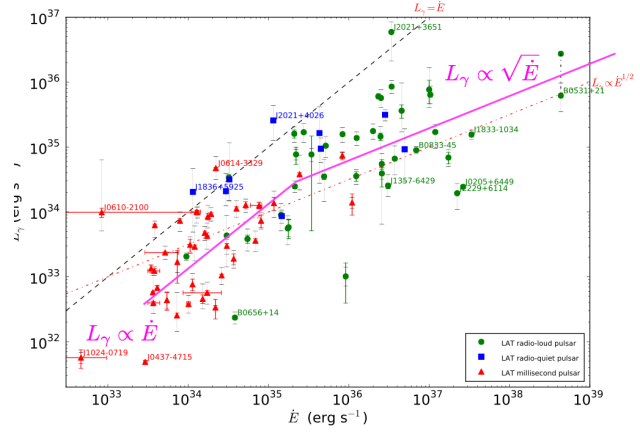


**Fig. 4** The proposed scaling of the  $L_\gamma(\dot{E})$  correlation is linear in the radiation reaction-limited regime (small  $\dot{E}$ ) and square root in the potential-limited regime (large  $\dot{E}$ ).

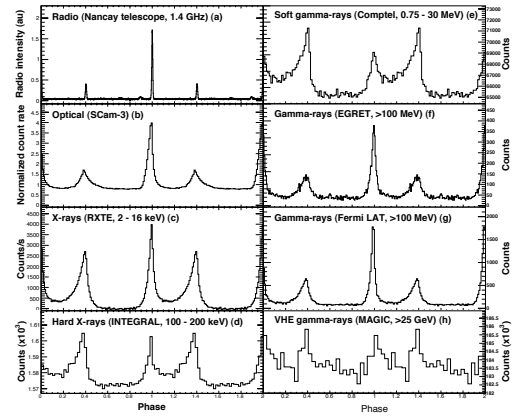


**Fig. 5** The average profile of the Crab pulsar from radio to  $\gamma$ -rays (from Abdo, 2010). The ratio of the interpulse to main pulse is repeated in the two spectral band: low in optical, increases to soft  $\gamma$ -rays, becomes low again in the MeV range and starts to increase again at GeV energies. In the IC model the two radiative components are expected to mirror each other.

soft UV photons that are scattered to GeV energies, and, formally, one expects UV-GeV correlation, X-rays and UV photons form a continuous spectral distribution and so one also expects X-ray - GeV correlation. One such correlation is well known: the ratio of MP to IP changes with energy and these changes are repeated in the two spectral bumps, Fig. 1

**Relating radio to high energy emission.** The present model of pulsar high energy emission requires that the emitting particles have a finite pitch angle. A possible excitation mechanism is related to the generation of the pulsar radio emission at the anomalous cyclotron resonance (Lyutikov et al., 1999). In this model the pulsar radio emission is produced directly by maser-type plasma instabilities op-

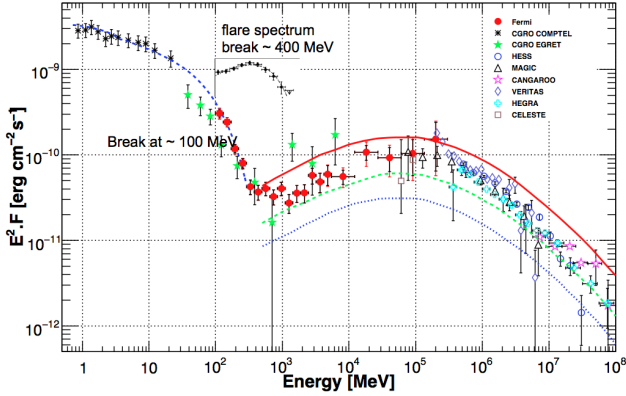


**Fig. 6** Crab spectrum with superimposed flare spectrum.

erating at the anomalous cyclotron-Cherenkov resonance  $\omega - k_{\parallel} v_{\parallel} + |\omega_B|/\gamma_{res} = 0$  (note the sign in front of the cyclotron term). At the anomalous resonance a particle emitting a wave undergoes a transition *up* (!) in Landau levels. Thus, initially one-dimensional distribution develops a finite pitch angle. As a result, resonant particles start emitting cyclotron photons at the normal cyclotron resonance.

Cyclotron motion of particles in the pulsar magnetosphere may be excited due to coherent emission of radio waves by streaming particles at the anomalous cyclotron resonance. Thus, a whole range of Crab non-thermal emission, from coherent radio waves to very high energy  $\gamma$ -rays - nearly eighteen decades in energy - may be a manifestation of inter-dependent radiation processes.

## 2 THE CRAB NEBULA GAMMA-RAY FLARES

The detection of flares from the Crab Nebula by AGILE and Fermi satellites (Buehler, 2012; Tavani, 2011), Fig. 6, is one of the most astounding discoveries in high energy astrophysics. The unusually short durations, high luminosities, and high photon energies of the Crab Nebula gamma-ray flares require reconsideration of our basic assumptions about the physics processes responsible for acceleration of (some) high-energy emitting particles in the Crab Nebula, and, possibly in other high-energy astrophysical sources. During flares, the Crab Nebula gamma-ray flux above 100 MeV exceeded its average value by a factor of several or higher (Abdo, 2011; Tavani, 2011), while in other energy bands nothing unusual was observed.

We associate the duration of the flare with stochastically changing local properties of plasma within the nebula. We envision flares originating from a highly localized emission region, so that the flare observables determine the intrinsic properties of the emission region, and not necessarily the overall bulk properties of the flow. The natural flaring

mechanism in this category is random relativistic magnetic reconnection events (Clausen-Brown & Lyutikov, 2012).

### Acceleration in PWNe: shocks and/or reconnection?

The discovery of flares from Crab Nebula challenges our understanding and particle acceleration in the PWNe. On the one hand, the low magnetization numerical models of Crab Nebula (Del Zanna et al., 2004; Komissarov & Lyubarsky, 2004) are able to reproduce the morphological details of the Crab Nebula down to intricate details. The implied acceleration mechanism is then the acceleration at the termination shock (Kennel & Coroniti, 1984; Rees & Gunn, 1974), presumably via the stochastic Fermi-type process. This is currently the dominant paradigm.

On the other hand, even before the discovery of Crab flares, Lyutikov (2010) argued that the observed cutoff in synchrotron spectrum of the Crab Nebula at  $\sim 100$  MeV in the persistent Crab Nebula emission is probably too high to be consistent with the stochastic shock acceleration. Indeed, balancing electrostatic acceleration in a regular electric field with synchrotron energy losses yields the synchrotron photon energy  $\epsilon_{\max} \sim \eta \hbar \frac{mc^3}{e^2} \approx 100$  MeV, where  $\eta$  is the ratio of electric to magnetic field strengths. Since high conductivity of astrophysical plasma ensures that in most circumstances  $\eta < 1$ , the observed value of the cutoff is right at the very limit. During the gamma-ray flares the cutoff energy approached even higher value of  $\sim 400$  MeV, suggesting Doppler boosting or a different acceleration mechanism. In addition, recent optical observations show no significant variability of the brightest features associated with the termination shock (Weisskopf, 2012), apparently ruling out the shock acceleration as a mechanism behind the flares.

Komissarov (2013); Lyubarsky (2012) pointed out that while particle acceleration may be efficient at the termination shock of the equatorial striped section of pulsar wind, it is unlikely to operate in the polar section which is free from stripes. Moreover, the magnetic dissipation is needed to reconcile the observed sub-equipartition magnetic field of the Crab Nebula with its theoretical models. This conclusion is supported by the recent numerical simulations Porth et al. (2013). Thus, low magnetization models reproduce the Crab PWN morphology, but the implied acceleration mechanism, the stochastic shock acceleration, fails to reproduce the spectrum.

Clausen-Brown & Lyutikov (2012) argued that the flares can be due to a highly localized emission region, or blob, so that the flare observables determine the intrinsic properties of the emission region. Magnetic reconnection provides a natural explanation of the implied relativistic motion discussed above, the intrinsic short timescales, and the flares' intermittency. Reconnection is a process in which the magnetic energy of a localized region, a current sheet, is suddenly converted to random particle energy, and bulk relativistic motion. Clausen-Brown & Lyutikov (2012) demonstrated that in the radiation reaction limit the electron distribution function may display a power-law with an excess, or pile-up, of particles near the synchrotron limit, in which



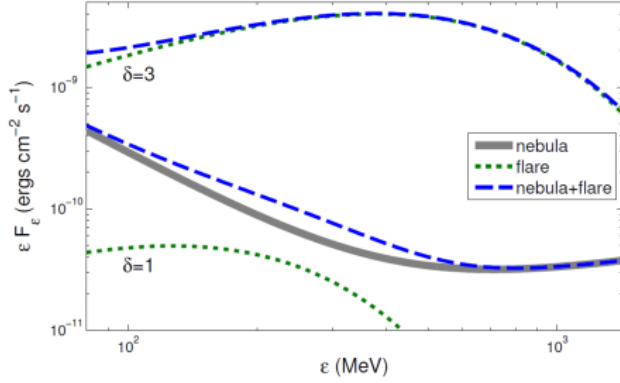


**Fig. 7** Doppler boosted single-particle synchrotron SEDs (dotted lines) for  $\delta = 1$  and  $\delta = 3$ . The average nebula SED (thick line) is summed with the flare SEDs to produce a combined SED shown by the dashed line.

case the emitting particles will display a SED that is close to the single-particle synchrotron SED. The observed spectrum of the flare is consistent with a mono-energetic pile-up Clausen-Brown & Lyutikov (2012).

Even a mild Doppler beaming can resolve the problem with the synchrotron upper limit. In Fig. 7 we have plotted the same small (total number of emitting electron  $\sim 10^{38}$ , produced by a pulsar within a second) intrinsic single-particle synchrotron SED with two different Doppler factors,  $\delta = 1$  and  $\delta = 3$ . The different Doppler factors affect the intrinsic SED's photon energies,  $\epsilon = \delta\epsilon'$ , and normalization,  $\epsilon F_\epsilon(\epsilon) = \delta^4 \epsilon' F'_\epsilon(\epsilon')$  (Lind & Blandford, 1985).

The non-detection of significant flaring by X-ray telescopes places a further constraint on the flare SEDs. If the flare SED comes from a mono-energetic electron distribution, then in the *Chandra* and *XMM-Newton* energy bands, the SED goes as  $\epsilon F_\epsilon \propto \epsilon^{4/3}$ . For the single-particle synchrotron SED, the X-ray variations are generally non-detectable.

**The minijet model.** We identify the flaring as reconnecting sites in the nebula plasma. The reconnection outflow speeds are then relativistic (Lyutikov & Uzdensky, 2003) and behave as “minijets,” a model that has been used to overcome the gamma-ray opacity problem in the context of gamma-ray bursts and active galactic nuclei (Lyutikov, 2006). We have constructed a statistical model of Crab Nebula high energy variability by assuming magnetic reconnection sites throughout the nebula are activated randomly, and once activated, display emission characteristics controlled by the reconnection outflow Doppler factor (Clausen-Brown & Lyutikov, 2012), Fig. 8. In our model, GeV flares are observed when a magnetically dominated site in the Crab nebula undergoes magnetic reconnection and launches a relativistic outflow that is, by chance, aligned with the line of sight. The observed flares’ unusually short durations and high luminosities suggest the emitting plasma is indeed moving toward Earth at relativistic speeds. Assuming shot-noise type generation of minijets, we can calculate observ-

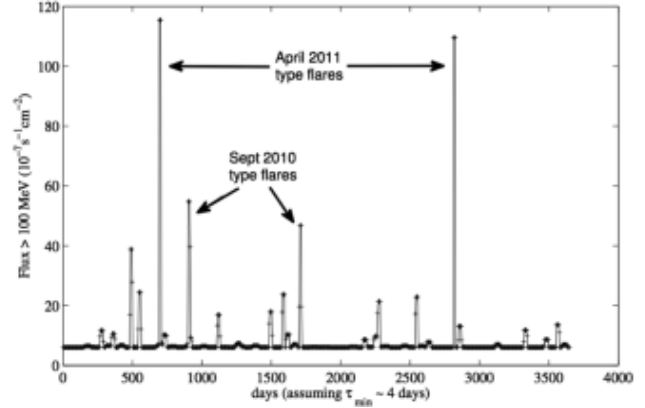


**Fig. 8** Monte-Carlo simulations of Crab Nebula flux variations with the minijet model. The minijet flux averaged over different flares is *dominated by rare bright flares*.

able quantities such as minijet timescale and flux distributions (Clausen-Brown & Lyutikov, 2012). Importantly, due to high powers dependence of the flux on Doppler beaming, the minijet flux averaged over different flares is *dominated by rare bright flares*. Another important statistical representation of the light curve is the power spectrum,  $P(\nu)$ , which measures its variability on different timescales: we predict  $P(\nu) \propto \nu^{-2}$  for sufficiently high frequencies.

The contradiction between low and high magnetization models described above calls into question the dominant mechanism of particle acceleration in PWNe via the stochastic shock acceleration and lends support to the alternative model, acceleration at relativistic reconnection events. If confirmed, this would be a *major paradigm change in high energy astrophysics as a whole*, since PWNe, and especially the Crab PWN, is used as prototypical source for studies of the high energy processes in the fields of Active Galactic Nuclei and Gamma Ray Bursts.

Reconnection physics is highly uncertain: it depends crucially on the kinetic and geometric properties of the plasma, which is very hard to test observationally. Often, various instabilities (based on inertial or cyclotron effects, on ions or electrons) often seem to account equally well (with astrophysical accuracy) for the observed phenomena. This situation may be contrasted with the shock acceleration schemes, where a qualitatively correct result for the spectrum of accelerated particles can be obtained from simple *macroscopic* considerations, the shock jump conditions (e.g., Blandford & Eichler, 1987).

We investigate the model in which high-energy particles are accelerated at localized reconnection events, e.g., on the equator or near the pole (Lyutikov, 2010). Previously, Clausen-Brown & Lyutikov (2012) showed that a statistical model of reconnection mini-jets is able to reproduce the observed intensity fluctuations. Clausen-Brown & Lyutikov (2012) argued that all of the high energy emission from the Crab nebula, both the nearly constant overall background and rare bright flares may be due to random stochas-

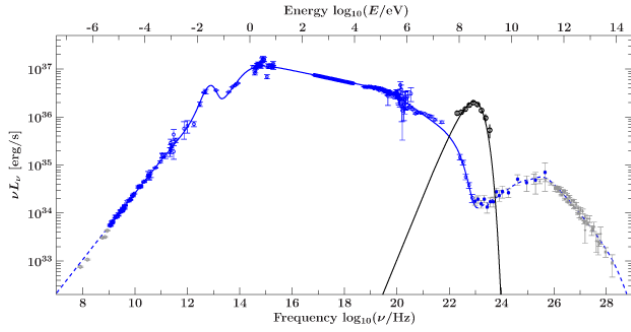


**Fig. 9** Overplotted are single electron SED and the *Fermi* flare data (black line and data) over data from a typical quiescent nebula spectrum and its model fit from Meyer et al. (2010).

tic reconnection events. They relied on the observation by Lyutikov & Uzdensky (2003) that in case of relativistic reconnection the outflow velocity may be relativistic - even mildly relativistic outflows, *e.g.*, with the Doppler factor of only a few, will produce high brightness variations due to the high-power dependence of the observed luminosity on the bulk motion. For a mono-energetic spectrum, the flares are easily missed at lower energies, Fig. 9.

The microphysics of the acceleration in relativistic reconnection layers has been previously addressed by Cerutti et al. (2012), who considered a *stationary* relativistic reconnection regime, following qualitatively the stationary Sweet-Parker model. But within the framework of stationary models of reconnection (*e.g.*, Lyubarsky, 2005; Lyutikov & Uzdensky, 2003) it is hard to achieve relativistic inflow velocities (Zenitani & Hoshino, 2007). We are developing a model of explosive collapse in a highly magnetized plasma, Fig. 10. The model has all the ingredients needed for Crab flares: explosive dynamics on Alfvén (light travel) time scale (starting from smooth initial condition), development of high electric field regions, with electric fields of the order of magnetic fields in the bulk and collimation of particles towards the low magnetic field regions.

## References

- Abdo, A. A. *et al.* . 2011, *Science*, 331, 739  
 Abdo, A. A. *et al.*. 2010, *ApJ*, 708, 1254  
 Blandford, R., & Eichler, D. 1987, *Phys. Rep.*, 154, 1  
 Buehler, R. 2012, *ApJ*, 749, 26  
 Cerutti, B., Uzdensky, D. A., & Begelman, M. C. 2012, *ApJ*, 746, 148  
 Clausen-Brown, E., & Lyutikov, M. 2012, *MNRAS*, 426, 1374  
 Daugherty, J. K., & Harding, A. K. 1982, *ApJ*, 252, 337  
 de Jager, O. C., , A. K., Michelson, P. F., Nel, H. I., Nolan, P. L., Sreekumar, P., & Thompson, D. J. 1996, *ApJ*, 457, 253  
 Del Zanna, L., Amato, E., & Bucciantini, N. 2004, *A&A*, 421, 1063

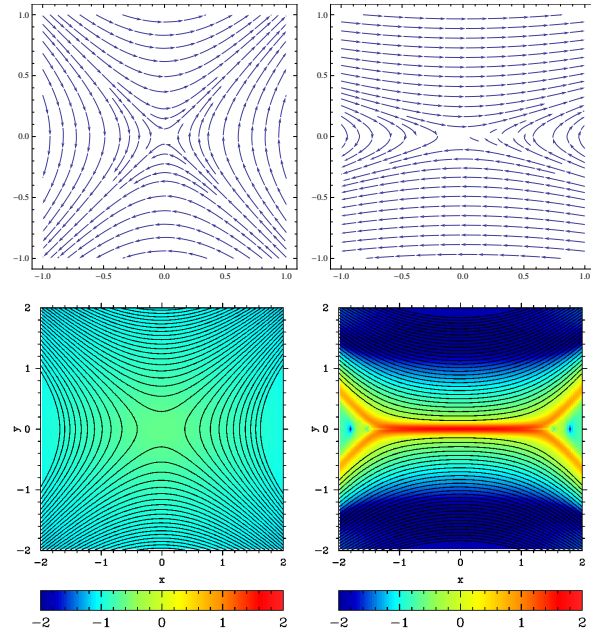


**Fig. 10** *Upper row.* Analytical structure of the magnetic field in the  $x - y$  plane during X-point collapse in force-free plasma. The initial configuration on the left is slightly “squeezed”. On dynamical time scale the X-point collapses to form a current sheet, right figure. *Lower row.* Numerical simulations of the X-point collapse (Komissarov, priv. comm.).

- Furth, H., Killeen, J., & Rosenbluth, M. N. 1963, *Phys. Fluid*, 6, 459  
 Harding, A. K., & Muslimov, A. G. 1998, *ApJ*, 508, 328  
 Kennel, C. F., & Coroniti, F. V. 1984, *ApJ*, 283, 694  
 Komissarov, S. S. 2013, *MNRAS*, 428, 2459  
 Komissarov, S. S., Barkov, M., & Lyutikov, M. 2007, *MNRAS*, 374, 415  
 Komissarov, S. S., & Lyubarsky, Y. E. 2004, *MNRAS*, 349, 779  
 Lind, K. R., & Blandford, R. D. 1985, *ApJ*, 295, 358  
 Lyubarsky, Y. E. 2005, *MNRAS*, 358, 113  
 —. 2012, *MNRAS*, 427, 1497  
 Lyutikov, M. 2003, *MNRAS*, 346, 540  
 —. 2006, *MNRAS*, 369, L5  
 —. 2010, *MNRAS*, 405, 1809  
 —. 2012, *ApJ*, 757, 88  
 —. 2013, *MNRAS*, 431, 2580  
 Lyutikov, M., Blandford, R. D., & Machabeli, G. 1999, *MNRAS*, 305, 338  
 Lyutikov, M., Otte, N., & McCann, A. 2012, *ApJ*, 754, 33  
 Lyutikov, M., & Uzdensky, D. 2003, *ApJ*, 589, 893  
 Meyer, M., Horns, D., & Zechlin, H.-S. 2010, *A&A*, 523, A2  
 Porth, O., Komissarov, S. S., & Keppens, R. 2013, *MNRAS*, 431, L48  
 Rees, M. J., & Gunn, J. E. 1974, *MNRAS*, 167, 1  
 Ruderman, M. A., & Sutherland, P. G. 1975, *ApJ*, 196, 51

- Tavani, M. e. 2011, *Science*, 331, 736  
The Fermi-LAT collaboration. 2013, ArXiv e-prints  
VERITAS Collaboration, & Aliu, E. e. 2011, *Science*, 334,  
69  
Weisskopf, M. C. e. 2012, ArXiv e-prints  
Zenitani, S., & Hoshino, M. 2007, *ApJ*, 670, 702  
Zhang, B., & Harding, A. K. 2000, *ApJ*, 532, 1150